

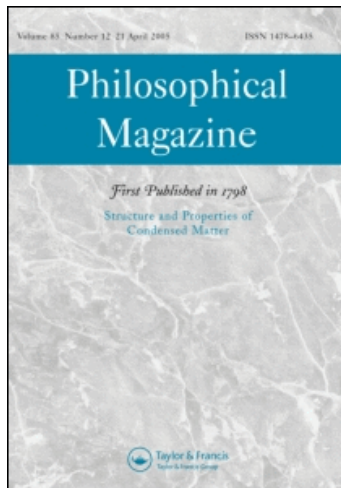
This article was downloaded by: [HEAL-Link Consortium]

On: 5 July 2010

Access details: Access Details: [subscription number 786636653]

Publisher Taylor & Francis

Informa Ltd Registered in England and Wales Registered Number: 1072954 Registered office: Mortimer House, 37-41 Mortimer Street, London W1T 3JH, UK



Philosophical Magazine

Publication details, including instructions for authors and subscription information:
<http://www.informaworld.com/smpp/title~content=t713695589>

The role of the recombination centers on the modulated photocurrent: Determination of the gap state parameters of semiconductors

M. Pomoni^a; A. Giannopoulou^a; P. Kounavis^a

^a Department of Engineering Sciences, School of Engineering, University of Patras, 26504 Patra, Greece

First published on: 25 June 2010

To cite this Article Pomoni, M. , Giannopoulou, A. and Kounavis, P.(2010) 'The role of the recombination centers on the modulated photocurrent: Determination of the gap state parameters of semiconductors', Philosophical Magazine,, First published on: 25 June 2010 (iFirst)

To link to this Article: DOI: 10.1080/14786435.2010.489031

URL: <http://dx.doi.org/10.1080/14786435.2010.489031>

PLEASE SCROLL DOWN FOR ARTICLE

Full terms and conditions of use: <http://www.informaworld.com/terms-and-conditions-of-access.pdf>

This article may be used for research, teaching and private study purposes. Any substantial or systematic reproduction, re-distribution, re-selling, loan or sub-licensing, systematic supply or distribution in any form to anyone is expressly forbidden.

The publisher does not give any warranty express or implied or make any representation that the contents will be complete or accurate or up to date. The accuracy of any instructions, formulae and drug doses should be independently verified with primary sources. The publisher shall not be liable for any loss, actions, claims, proceedings, demand or costs or damages whatsoever or howsoever caused arising directly or indirectly in connection with or arising out of the use of this material.

The role of the recombination centers on the modulated photocurrent: Determination of the gap state parameters of semiconductors

M. Pomoni, A. Giannopoulou and P. Kounavis*

*Department of Engineering Sciences, School of Engineering, University of Patras,
26504 Patra, Greece*

(Received 20 December 2009; final version received 19 April 2009)

Exact expressions for the out of phase modulated photocurrent (MPC), the so-called Y signal, with a clear physical insight for density of states (DOS) spectroscopy are derived without any approximation. It is found that, apart from the capture rate of the majority carriers into the probed gap states, additional mixed contributions from the recombination processes of the free majority carriers with trapped minority carriers may be important for the Y signal of lower frequencies. These additional contributions prevent the extraction of a reliable DOS. They become important as long as the capture coefficient for the majority carriers of the recombination centers, where the minority carriers are trapped, is comparable to or higher than that of the recombination centers were the majority carriers are trapped. In this case, the recombination rate is relatively high and the mixed contributions from the recombination processes can be detectable in the experimental Y signal and may also induce a phase lead. Taking advantage of this behavior it can be experimentally verified when these recombination processes are negligible in order to safely extract the accurate DOS parameters.

Keywords: semiconductors; photoelectrical modelling; numerical simulation; thin films

1. Introduction

The modulated photocurrent (MPC) technique has been applied to determine the density of states (DOS) in the energy gap of various semiconductors including crystalline [1–3], amorphous [4–10], microcrystalline [11], quasicrystalline [12], as well as organic [13,14] semiconductors. This technique is very powerful as it can reveal even very low trap densities, as well as the capture coefficients. The experimental setup, as shown in the sketch of Figure 1a, is simple and requires relatively cheap equipment. In this experiment, a semiconductor film with ohmic electrodes in coplanar geometry is illuminated by two light emitted diodes (LEDs) of bandgap light. One LED provides relatively weak sinusoidally modulated light (see Figure 1b) of angular modulation frequency ω generating the MPC. The second

*Corresponding author. Email: pkounavis@des.upatras.gr

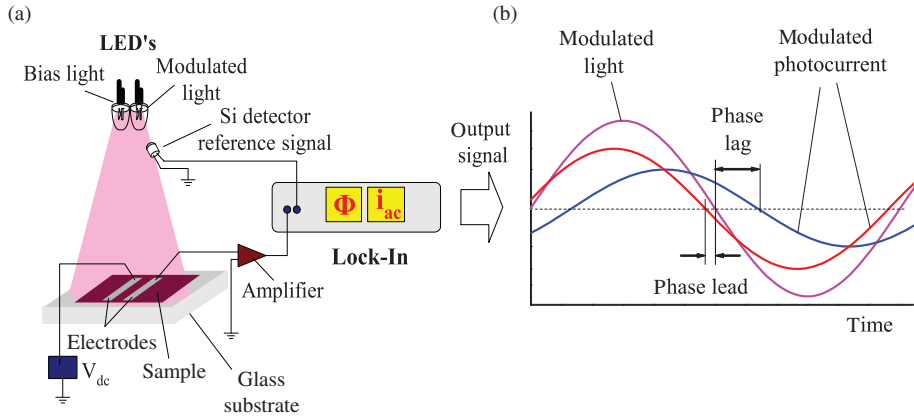


Figure 1. Sketch showing the experimental setup of the MPC experiment in (a) and evolution with time of the modulated light and the amplitude of the MPC i_{ac} in (b), where the phase shift is illustrated, which may be a phase lag or a phase lead.

LED provides moderate bias light generating a constant photocurrent. The MPC is amplified by a low noise current amplifier close to the sample to minimize stray capacitance. The output from the amplifier is analyzed by a lock-in amplifier, which provides the amplitude, i_{ac} , of the MPC and the phase shift, ϕ , between the MPC and the modulated light (see Figure 1b), which may be a phase lag [1,5–8] or a small phase lead [15]. The theoretical analysis of the MPC data is based on the multiple trapping model, and the derived basic expressions indicate two different regimes: that at high frequencies (ω) and/or low bias light levels, the so-called high frequency (HF) or emission-limited regime; and that at low frequencies and/or high bias light levels, the so-called low frequency (LF) or trapping-limited regime.

Simple theoretical expressions giving physical insight into the MPC data were originally presented in 1981 by Oheda [1] for the HF regime, which is typically a small portion of the experimental spectra at higher ω . Based on this analysis, Bruggemann et al. [6] in 1990 proposed a formula for the determination of the so-called reduced DOS (r-DOS), $(c/\mu)D(E_\omega)$. This formula provides, by means of the i_{ac} and ϕ data, the r-DOS at the probe energy level E_ω for which the thermal emission rate of the majority carriers equals the modulation frequency ω . Thus, by scanning ω [8,16–18] the DOS at different E_ω levels can be obtained. This method is applicable exclusively to the MPC data in the HF regime. Various attempts have been made to extract information about the DOS and to determine the usually unknown ratio of the capture coefficient to the mobility of the predominated carriers, c/μ , by means of the MPC data of lower ω [9,19–30]. However, the general analytical expressions originally derived by Longeaud and Kleider [19] in 1992 and Hattori et al. [20] in 1994 are very complicated when extracting a simple relation between the MPC of lower ω and the DOS. For this reason an empirical expression was derived by Hattori et al. [20] which was applied to determine the DOS parameters of a-Si:H by means of the MPC data obtained upon scanning the bias light level. During this scan the probe energy level (E_ω) was assumed *a priori* fixed. Subsequently, in 2001 we presented a general theoretical analysis of the MPC [31] where it was shown that the

E_ω level can be shifted not only by the modulation frequency, but also by the bias light level. This result invalidates [32] the basic assumption of the method of Hattori et al. In our theoretical analysis [31], a simple approximate expression for the out of phase MPC signal, the so-called Y signal, was extracted. The Y signal was approximated by the capture rate of the majority carriers into the probed gap states for any frequency. This is the basis of our DOS spectroscopy, which has the advantage that it can be used to extract the capture coefficients and the density of the probed states by means of the i_{ac} and ϕ data for any ω , including those at lower ω which were not utilized before [32–36]. Later, in 2002, Koropecki et al. [37] of the INTEC group and in 2004 Guenier et al. [38] of the LGEP group concentrated their analysis on the LF regime in which the expressions for the MPC take a relatively simpler form. They arrived to similar approximate formulas differing in the proportionality constant for the calculation of the DOS.

The above mentioned methods are based on specific assumptions which result in different simplified approximate expressions relating to the MPC data with a specific probed DOS. However, the validity and the limitations of these approximations have not been extensively explored. Moreover, it was not specified when a reliable DOS can be extracted from a given set of MPC data. Recently, different studies have been devoted to the accuracy of the DOS determined from the MPC data by means of model simulations [39–42]. It was deduced that the capture coefficients of the gap states are important for the MPC, without exactly understanding their role [42]. Moreover, an unexplained phase lead has been obtained both experimentally and by simulations [15].

This work concerns a theoretical analysis of the MPC concentrated on these issues. Specifically, simple exact analytical expressions are derived in Section 2, without any approximation, describing all the physical processes contributing to the MPC. It is demonstrated when and how the accurate gap state parameters can be safely extracted from a given set of MPC data. All the theoretical predictions are confirmed by means of model simulations in Section 3 and compared with experimental observations in Section 4.

2. Theoretical analysis

2.1. Basic expressions

The expressions for the free electron and hole modulated densities n_{ac} and p_{ac} , respectively, have been extracted in our first analysis and are given by Equations (B3) and (B4) of [31], respectively. It has proved convenient to express them in the form $n_{ac} = G_{ac}/(X_n + jY_n)$ and $p_{ac} = G_{ac}/(X_p + jY_p)$, where j is the imaginary unit, $Y_{n,p}$ and $X_{n,p}$ are the imaginary and real parts of the denominators of Equations (B3) and (B4) of [31] and G_{ac} is the modulated light generation rate. The experimental i_{ac} , ϕ data, which are expressed in terms of the real and imaginary parts of n_{ac} and p_{ac} (see Equations (24) and (25) of [31]), can be used to directly calculate the Y signal by means of

$$Y = \mu e G_{ac} \frac{\sin \phi}{\sigma_{ac}}, \quad (1)$$

where μ is the mobility of the predominant carriers and σ_{ac} is the modulated photoconductivity calculated from i_{ac} . The so-calculated Y signal from the experimental data is the essential parameter of the MPC experiment, because it may be directly proportional to the probed DOS ($D(E_\omega)$) for any frequency [31].

Specifically, we have shown that the Y signal may coincide with the imaginary part Y_n (Y_p), when electrons (holes) dominate. Unfortunately, only an approximate expression for the above imaginary part has been obtained in our first analysis [31] relating the Y signal with the probed DOS ($D(E_\omega)$). Here the exact expression for this imaginary part is obtained without any approximation. For this purpose, several species of monovalent gap state $D^i(E)$ distributions are considered with different capture coefficients c_n^i and c_p^i for the electrons and holes, respectively. This is because the energy gap consists of gap states of different origin, whereas the charge state of a given localized state is altered following capture of a carrier. The electrons are assumed, throughout this analysis, as the majority carriers. Hence we concentrate on the exact expression for the Y_n , which is the imaginary part of the denominator of the exact expression for n_{ac} of Equation (B3) of [31] derived without any approximation. For this purpose, the factor K , which is given by Equation (23) in the Appendix and appears in the exact expression for n_{ac} , is replaced by its imaginary K_{im} and real K_{re} parts. The derived Y_n is expressed by three components as

$$Y_n \cong Y_{1n} + Y_{2n} + Y_{3n}, \quad (2)$$

where

$$Y_{1n} = \sum_i \int_{E_V}^{E_C} d_n^i(E) b_{\omega n}^i(E) c_n^i D^i(E) dE, \quad (3)$$

$$Y_{2n} = \sum_i \int_{E_V}^{E_C} d_n^i(E) g^i(E) b_{\omega p}^i(E) c_p^i D^i(E) dE, \quad (4)$$

$$Y_{3n} = \sum_i \int_{E_V}^{E_C} d_n^i(E) q_n^i(E) c_n^i D^i(E) dE. \quad (5)$$

In Equations (3)–(5) the following functions appear:

$$b_{\omega n}^i(E) = \frac{\omega r_n^i(E)}{\omega^2 + [S^i(E)]^2}, \quad (6)$$

$$b_{\omega p}^i(E) = \frac{\omega r_p^i(E)}{\omega^2 + [S^i(E)]^2}, \quad (7)$$

$$d_n^i(E) = \frac{nc_n^i + r_n^i(E)}{S^i(E)}, \quad (8)$$

$$q_n^i(E) = \frac{\omega c_p^i [ng^i(E) + p]}{\omega^2 + (S^i(E))^2}, \quad (9)$$

$$g^i(E) = K_{im} S^i(E) / \omega - K_{re}. \quad (10)$$

Here we have $S^i(E) = nc_n^i + pc_p^i + r_n^i(E) + r_p^i(E)$, where $r_n^i(E) = c_n^i N_C kT \times \exp[-(E_C - E)/kT]$ and $r_p^i(E) = c_p^i N_V kT \exp[-(E - E_V)/kT]$ are the thermal emission rates of the electrons and holes, respectively, from a gap energy level E , and kT is the thermal energy. E_V and E_C are the conduction and valence band edges, where the effective DOS is N_C and N_V , respectively. The above exact expressions are appropriate to reveal all the physical processes involved in the Y_n and to clarify when it is possible to extract a reliable DOS, as explained below.

2.2. The cases where DOS spectroscopy is possible

In the present analysis, it is assumed that the mobility-lifetime product of electrons is much higher than that of holes $\mu_n \tau_n \gg \mu_p \tau_p$ and $n \gg p$, such that $nc_n^i \gg pc_p^i$. Moreover, it is assumed that $Y \cong Y_n$, which is obtained as long as the mobility capture time product of the majority carriers is much higher than that of minority carriers [42]. This way, our analysis is concentrated on the Y_n . A similar analysis holds for the Y_p as long as holes predominate and $Y \cong Y_p$.

The gap states having the higher relative contribution to the Y_n for any frequency are defined by the products $d_n^i(E)b_{on}^i(E)$, $d_n^i(E)b_{op}^i(E)$ and $\omega/(\omega^2 + [S^i(E)]^2)$ which appear in Y_{1n} , Y_{2n} and Y_{3n} of Equations (3)–(5), respectively. These products are illustrated graphically in Figures 2a and b, for various modulation frequencies ω by taking $nc_n^i = 99 \text{ s}^{-1}$ and $pc_p^i = 1 \text{ s}^{-1}$, which give a characteristic frequency $\omega_t^i = nc_n^i + pc_p^i = 100 \text{ rad s}^{-1}$.

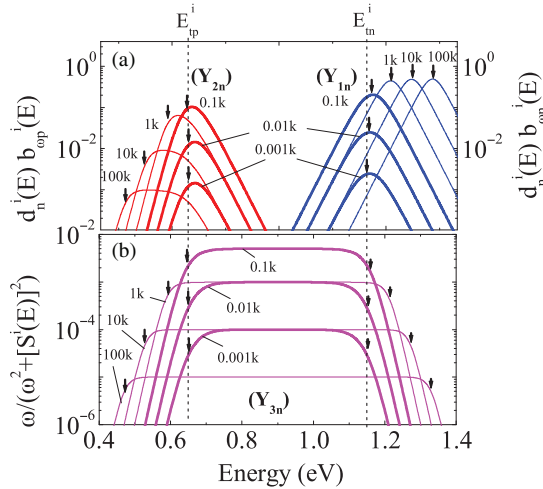


Figure 2. Energy dependence of the $d_n^i(E)b_{on}^i(E)$ (right axis) and $d_n^i(E)b_{op}^i(E)$ (left axis) products above and below midgap, respectively, in (a) and of the $\omega/(\omega^2 + [S^i(E)]^2)$ ratio in (b) for various ω indicated by the numbers in units of $k = 1000 \text{ rad s}^{-1}$. These products define the gap states with the higher relative contribution to each component of Y_n indicated in parentheses. The characteristic frequency is at $\omega_t^i = 100 \text{ rad s}^{-1}$ and $c_n^i = c_p^i = 1 \times 10^{-8} \text{ cm}^3 \text{ s}^{-1}$. The arrows above and below midgap indicate the E_{on}^i and E_{op}^i levels, respectively. Thinner and thicker lines correspond to $\omega > \omega_t^i$ and $\omega \leq \omega_t^i$, respectively.

As demonstrated in Figure 2a (right axis), the first Y_{1n} component is dominated by the capture rate, $c_n^i D^i(E) dE$, of electrons into the gap states centered at a frequency dependent energy level above midgap. This is the so-called probe energy level of electrons $E_{\omega n}^i$ defined by the respective maximum of the sharply peaked $b_{\omega n}^i(E)$ function of Equation (6) and is given by

$$E_C - E_{\omega n}^i = kT \ln \left[\frac{c_n^i N_C kT}{(\omega^2 + \{\omega_i^j\}^2)^{1/2}} \right]. \quad (11)$$

The $b_{\omega n}^i(E)$ function effectively selects the gap states around the $E_{\omega n}^i$ where the thermal emission rate $r_n^i(E)$ equals the modulation frequency ω . Thus the $D^i(E_{\omega n}^i)$ density gives the largest contribution to the Y_{1n} and to the quadrature component of the MPC. As a result, a delay of the MPC from the modulated light with a phase lag (see Figure 1b) is obtained, due to the trapping and thermal release of the electrons into and from probed states at $E_{\omega n}^i$. The gap states shallower and deeper than $E_{\omega n}^i$ emit trapped electrons faster and slower, respectively, during the modulation period and do not contribute to the phase lag. In the HF regime, where $\omega \gg \omega_i^j$, the $E_{\omega n}^i$ level according to Equation (11) shifts by the modulation frequency ω to shallower energies from the trap quasi-Fermi level of trapped electrons E_{in}^i . In the LF regime, where $\omega \ll \omega_i^j$, Equation (11) predicts that the $E_{\omega n}^i$ level is fixed at the E_{in}^i level, which is defined by $r_n^i(E_{in}^i) = \omega_i^j$. In the HF regime, Y_{1n} is the only important component and facilitates DOS spectroscopy. In the LF regime, the other two components Y_{2n} and Y_{3n} may also become important.

The gap states with the predominant contribution in Y_{2n} for the LF regime are mainly selected by the sharply peaked $b_{\omega p}^i(E)$ function. These states are shown in Figure 2a (thick lines below midgap) and they are centered at the trap quasi-Fermi level of holes E_{ip}^i , where $r_p^i(E_{ip}^i) = \omega_i^j$. In addition, Y_{2n} from Equation (4) is proportional to the $g^i(E)$ of Equation (10), which contains the real and the imaginary parts of K . By considering that both of these parts, according to Equations (25) and (26) of the Appendix, are proportional to the ratio p/n and using Equation (8), then Y_{2n} for $\omega \ll \omega_i^j$ is found to be proportional to the $c_n^i p c_p^i / S^i(E) D^i(E) dE$ rate. Since the ratio $p c_p^i / S^i(E)$ gives the fraction of the unoccupied states, the above rate indicates that Y_{2n} is proportional to the recombination rate of free electrons with the trapped holes in the gap states around the E_{ip}^i level. Similarly, in Equation (5), by taking into account Equation (9) and Equations (25) and (26) of the Appendix, then Y_{3n} for the LF regime is also found to be proportional to the $c_n^i p c_p^i / S^i(E) D^i(E) dE$ rate. The above rate indicates that Y_{3n} is proportional to the recombination rate of free electrons with trapped holes in the recombination centers of the $D^i(E)$ distributions between E_{ip}^i and E_{in}^i . These centers, as is evident from Figure 2b (thick lines), are selected by the ratio $\omega / (\omega^2 + [S^i(E)]^2)$ in Equation (9) and they give the largest contribution to Y_{3n} . This way, the recombination processes involved in Y_{2n} and Y_{3n} may complicate the extraction of a DOS from the data in the LF regime.

It is obvious that this difficulty may be overcome and an absolute DOS can be extracted by utilizing all the MPC data, as long as the Y_{1n} component predominates in the Y_n and Y signal, not only for the HF regime but also for any ω . This way, the probed $D(E_{\omega n})$ dominating in Y_{1n} can be extracted directly from the Y signal. It is worth mentioning that this possibility can be tested experimentally, because Y_{1n} has

the well-defined frequency dependence of the capture rate $1/\tau_{\omega n}$ of electrons into the probe $E_{\omega n}$ level according to

$$Y \cong Y_{1n} \cong \frac{1}{\tau_{\omega n}} = \frac{\pi}{2} H(\omega, \omega_t) c_n D(E_{\omega n}) kT. \quad (12)$$

This relation is obtained from Equation (3) by considering that Equation (8), for all the probe $E_{\omega n}$ levels, gives $d_n^i(E) \cong 1$ for $nc_n^i \gg pc_p^i$ and that the weighting function $b_{\omega n}^i(E)$ can be replaced by a delta function. Equation (12) has already been derived in our first analysis [31] for the Y_n using an approximation, as is clarified in Section 2.4. In Equation (12), the so-called universal H function is given by $H(\omega, \omega_t) = 1 - (2/\pi) \arctan(\omega_t/\omega)$, which has a step at ω_t . This step generates, ultimately, a step in the Y signal with a characteristic decay at low ω which can be used to verify Equation (12) experimentally. This decay is due to the fact that the electrons interacting with the probed states at $E_{\omega n}$, which is practically the E_m level at low ω , have an increasingly longer time with decreasing ω to thermal release to the conduction band during a modulation period. This effect results in a decrease of the Y signal and phase shift. Specifically, if $Y \cong Y_{1n}$, then in the HF regime ($\omega \gg \omega_t$) we have $H(\omega, \omega_t) \cong 1$, so that according to Equation (12) all the experimental Y spectra of different bias light levels should merge in the bias light intensity-independent spectrum of $Y_0 \cong \frac{\pi}{2} c_n D(E_{\omega n}) kT$. The experimental Y signal with decreasing ω should start to drop around ω_t from the values of Y_0 following the characteristic decay of the $1/\tau_{\omega n}$ rate, due to the step of the H function [31]. This prediction can be verified experimentally, because all the parameters c_n , ω_t and $D(E)$ required to calculate the $1/\tau_{\omega n}$ rate from Equation (12) can be reconstructed from the experimental Y spectra, without any *a priori* assumption about the DOS. This is illustrated in Section 3.4 by means of simulation examples.

2.3. The effect of recombination on the Y signal

In the previous section, it was deduced that the contributions from the recombination processes governing Y_{2n} and Y_{3n} should have a negligible contribution to the Y signal, in order for the condition of Equation (12) to be valid and to extract the DOS. It is then very important to specify the appropriate DOS parameters of the recombination centers which minimize these recombination processes. The exact role of the recombination centers to the dc photoconductivity and MPC can be better clarified by means of a simple DOS model with one valence band-tail like gap state distribution $D^v(E)$ below E_F and another conduction band-tail like gap state distribution $D^c(E)$ above E_F . It is also considered that E_F lies on the minimum where the $D^v(E)$ and $D^c(E)$ overlap, so that these distributions above and below E_F , respectively, vanish and are neglected. This way, it is possible to distinguish the exact role of the characteristics of each $D^v(E)$ and $D^c(E)$.

The charge neutrality condition states that the density of the trapped electrons above E_F equals the density of the trapped holes below E_F . By neglecting the thermal emission rates this becomes

$$\frac{nc_n^c}{nc_n^c + pc_p^c} N_r^c = \frac{pc_p^v}{nc_n^v + pc_p^v} N_r^v, \quad (13)$$

where $N_r^c = \int_{E_F}^{E_{in}} D^c(E)dE$ and $N_r^v = \int_{E_{tp}}^{E_F} D^v(E)dE$. It is obvious that the free carrier densities n, p are adjusted to fulfill the above condition, depending on the density of the recombination centers, as well as their capture coefficients. This is more evident from $n/p = (c_p^v/c_n^v)(N_r^v/N_r^c)$ which results from Equation (13) for $nc_n^i \gg pc_p^i$. An important parameter for the photoelectric properties of a photoconductor is the recombination rate, R , which, in steady state, equals the dc generation rate, G_{dc} , according to

$$R = G_{dc} = \frac{nc_n^v pc_p^v}{nc_n^v + pc_p^v} N_r^v + \frac{nc_n^c pc_p^c}{nc_n^c + pc_p^c} N_r^c. \quad (14)$$

The first and second terms in the right hand side of the above relation indicate that R can be expressed by the capture rate, n/τ_n^v , of the free electrons into the trapped holes below E_F and by the capture rate, p/τ_p^c , of the free holes into the trapped electrons above E_F , respectively, as shown schematically in Figure 3. The first rate dominates, namely, $n/\tau_n^v \gg p/\tau_p^c$, because $nc_n^i \gg pc_p^i$. Therefore, most of the recombination traffic is taking place through the recombination centers below E_F (down arrows in Figure 3), which is practically governed by the c_n^v for a given DOS. By incorporating Equation (13) in Equation (14) the lifetimes of electrons and holes defined by $\tau_n = n/G_{dc}$ and $\tau_p = p/G_{dc}$, respectively, are

$$\tau_n = \frac{1}{C_e c_n^c N_r^c}, \quad (15)$$

$$\tau_p = \frac{1}{c_p^v N_r^v}. \quad (16)$$

Thus for a given DOS the capture coefficient, c_n^v , for electrons of the recombination centers where the minority carriers are trapped determines, through the parameter $C_e = c_n^v/c_n^c$, the lifetime of electrons τ_n , the photosensitivity [45] and the recombination rate, which is written as

$$R = C_e nc_n^c N_r^c. \quad (17)$$

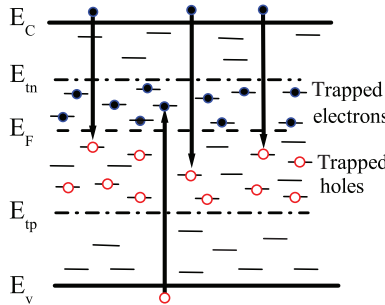


Figure 3. Recombination processes involving capture of free electrons by trapped holes (down arrows) and capture of free holes by trapped electrons (up arrows). The first process dominates recombination, as the densities of trapped electrons and holes are equal and $nc_n^i \gg pc_p^i$.

Note that, although c_p^v affects the p density, it has no net effect on R and Y_n , because the changes in c_p^v are counteracted by the induced changes in p . Equations (15) and (16) agree with the respective lifetimes of Simmons–Taylor theory [43], except for the parameter C_e in Equation (15). This parameter is absent in the respective expression of the original Simmons–Taylor theory, because these authors considered constant capture coefficients ($c_n^v = c_n^c$) so that $C_e = 1$.

The approximate Equations (25) and (26) for K_{im} and K_{re} , derived in the Appendix for the LF regime, are incorporated in Equations (4) and (5) in order to obtain simplified expressions for Y_{2n} and Y_{3n} . Indeed, by means of the charge neutrality condition of Equation (13) it is found that the total contribution of Y_{2n} and Y_{3n} can be expressed by the first component Y_{1n} as $Y_{2n} + Y_{3n} \cong -(C_e/2)Y_{1n}$. This relation indicates that the total contribution of Y_{2n} and Y_{3n} is governed by C_e . This is reasonable, because Y_{2n} and Y_{3n} are proportional to the recombination rates of free electrons with trapped holes in recombination centers and these rates, according to Equation (17), are governed by C_e . Moreover, the net total $Y_{2n} + Y_{3n}$ contribution appears negative, which indicates that the recombination processes involved in Y_{2n} and Y_{3n} are associated with a phase lead. Therefore, in the LF regime, Y_n depends on the ratio of the capture coefficients for the majority carriers $C_e = c_n^v/c_n^c$ according to the simple relation

$$Y \cong Y_n \cong \left(1 - \frac{C_e}{2}\right) Y_{1n}, \quad (18)$$

which is verified by means of simulations in Section 3.3 for $nc_n^i \gg pc_p^i$. Similar arguments can be made for Y_p , as long as holes are the majority carriers. In this case, the crucial parameter is $C_h = c_p^c/c_p^v$.

Therefore, for $C_e \ll 2$ the recombination rate is sufficiently low and according to Equation (18) the recombination processes involved in Y_{2n} and Y_{3n} are kept practically negligible to Y_n for the LF regime as well. This results in the condition of Equation (12), allowing DOS spectroscopy. By contrast, for $C_e > 2$ according to Equation (18) the negative total contribution from the recombination processes involved in Y_{2n} and Y_{3n} dominates, giving rise to a negative sign for the Y_n and Y signal and a phase lead (see Figure 1b). A phase lead has also been reported by other authors by means of experimental data [15] and simulation, without clarifying the exacting underlying mechanism [40].

2.4. Comparison with previous analysis

The second Y_{2n} and third Y_{3n} components of the imaginary part Y_n of the majority carriers derived in the present analysis are missing from our first theoretical analysis [31]. This is because it was considered that the factor K defined by Equation (23) in the Appendix, which is important only for the expressions for the MPC in the LF regime, can be approximated by the ratio of the free carrier dc densities p/n , whereas its imaginary part was neglected. Note that these approximations are supported by Equations (25) and (26) of the Appendix. By incorporating the above approximations, $K_{\text{re}} = p/n$ and $K_{\text{im}} = 0$, in the exact Equations (4) and (5), then Y_{2n} and Y_{3n} in the LF regime become zero. This way, Y_n is described practically by Y_{1n} of

Equation (12), which was also deduced in our first analysis. However, K_{re} , according to Equation (25), may be slightly higher or lower than the ratio p/n for which Equation (5) gives a finite value for Y_{3n} . In addition, although K_{im} in the LF regime is negligible compared to K_{re} , the contribution of K_{im} in Equations (4) and (5) could always be not negligible. This is due to the fact that K_{im} appears in the above equations as a product with the ratio $S^i(E)/\omega$. This product, taking into account the expression for K_{im} of Equation (A4) in the Appendix, may not be negligible. Hence the above approximations adopted in our first analysis may not be sufficient to provide a negligible contribution of $Y_{2n} + Y_{3n}$ to Y_n at low ω .

In fact, as deduced above, C_e is the crucial parameter and $C_e \ll 2$ is required to minimize the contribution of the recombination processes of Y_{2n} and Y_{3n} to Y_n and Y . This important role of C_e was not recognized in our first analysis. For simplicity, the Y signal was simulated for $C_e = 1$ and as a first approximation it was taken in agreement with $1/\tau_{\omega n}$ of Equation (12), which in fact is a better approximation for $C_e < 1$ according to Equation (18) and our recent simulations [42]. In any case, Equation (12), which is the essential restriction of our DOS spectroscopy, should be verified experimentally, in order to safely extract the accurate DOS by means of the general formula extracted in our previous analysis from Equation (12) [31]:

$$D(E_\omega) \cong \frac{2}{\pi} \frac{(Y/\mu)\sigma_p}{e\omega_t H(\omega, \omega_t) kT}. \quad (19)$$

The absolute capture coefficient for the majority carriers can be calculated from $c = e\omega_t\mu/\sigma_p$ by means of the characteristic frequency ω_t , which is extracted according to the procedure described before [31], and the measured dc photoconductivity σ_p , by considering that $\omega_t \cong nc_n$ ($\omega_t \cong pc_p$) when electrons (holes) dominate. The c so derived can be incorporated in Equation (11) to obtain the probed trap depths E_ω

$$E_\omega = kT \ln \left[\frac{(e\omega_t/\sigma_p)\mu N_0 kT}{(\omega^2 + [\omega_t]^2)^{1/2}} \right], \quad (20)$$

for any ω , by introducing the value for the μN_0 product, where N stands for N_C or N_V .

The analysis originally proposed by the LGEP group [38] and later adopted by the INTEC group is, for simplicity, based on the hypothesis that the capture coefficients of the gap states for the electrons and holes in the entire energy gap are the same, corresponding to $C_e = 1$. For $C_e = 1$, Equation (18) reduces to

$$Y \cong Y_n \cong Y_{1n}/2. \quad (21)$$

In the LF regime, a series expansion of the function H to first order gives $H(\omega, \omega_t^i) \cong \frac{2}{\pi} (\frac{\omega}{\omega_t^i})$. In addition, the phase shift, ϕ , is small so that $\tan \phi \cong \sin \phi$ and $G_{ac}/G_{dc} \cong \sigma_{ac}/\sigma_{dc}$. By introducing these approximations into our Equation (19) and using Equations (1), (12) and (21), we arrive at the simple approximate formula

$$D(E_t) \cong 2 \frac{G_{dc}}{kT} \frac{\tan \phi}{\omega}, \quad (22)$$

which was proposed by the LGEP group for DOS spectroscopy. This formula, using all the phase shift (ϕ) data in the LF regime, gives a single density, which is the DOS, $D(E_t)$, at the quasi-Fermi level of the trapped majority carriers, E_t . This density differs from that calculated with our Equation (19) using all the i_{ac} and ϕ data in the LF regime by a factor of 2, due to the factor of 2 in Equation (21), which is the essential restriction of this method. However, this restriction (obtained with $C_e = 1$) cannot be tested experimentally and the actual DOS cannot be obtained from Equation (22) in the cases of $C_e < 1$ and $C_e > 1$.

3. Model simulations

3.1. Details of simulations

In this section, model simulations are employed in order to verify the theoretical predictions of the previous sections, rather than to fit particular experimental spectra. Moreover, the MPC data generated by the simulations serve as possible experimental data in which our methods are applied to illustrate when, and how safely, information about the DOS parameters can be extracted. For this purpose we consider the simple DOS model of Figure 4 with the $D^v(E)$ and $D^c(E)$ distributions. These distributions include exponential valence and conduction band-tails with characteristic energies of $E_{ov} = 55$ and $E_{oc} = 35$ meV, respectively. In addition, $D^v(E)$ and $D^c(E)$ include Gaussian distributions, having a maximum density of $3 \times 10^{17} \text{ cm}^{-3} \text{ eV}^{-1}$ at 0.56 eV and $1 \times 10^{16} \text{ cm}^{-3} \text{ eV}^{-1}$ at 1.28 eV with half-width at half maxima of 0.15 eV and 0.2, respectively. The energy gap is 1.8 eV and the Fermi level is slightly above midgap at 1.0 eV. In this model, $D^v(E)$ and $D^c(E)$ rapidly vanish above and below E_F , respectively. This way, it is possible to examine the crucial role of the capture coefficient of the recombination centers below and above E_F to the MPC, predicted in Section 2.3. The capture coefficients are taken as $c_p^v = 10c_n^v = 1 \times 10^{-7} \text{ cm}^3 \text{ s}^{-1}$ and $c_n^c = 10c_p^c = 1 \times 10^{-7} \text{ cm}^3 \text{ s}^{-1}$ corresponding to negatively ($D^v(E)$) and positively ($D^c(E)$) charged centers, respectively. This model assures that the electrons are the majority carriers, giving $n \gg p$ such that $nc_n^i \gg pc_p^i$. The effect of the C_e parameter on the Y signal predicted in Section 2 is studied by changing c_n^v , keeping the rest of the parameters fixed.

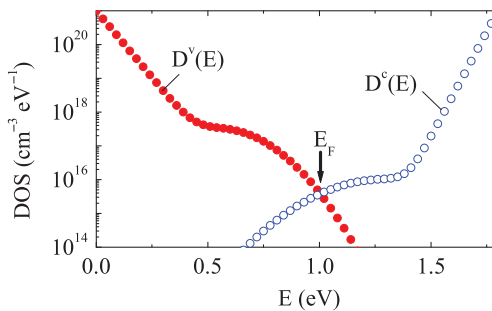


Figure 4. Gap state distributions $D^v(E)$ (solid circles) and $D^c(E)$ (open circles) of the DOS model introduced in the simulations.

The simulations were conducted for a fixed temperature of 300 K. Specifically, for a given free electron density n , the respective density p of free holes is numerically obtained by means of the charge neutrality condition [31,43,44]. The exact Y spectrum is calculated from Equation (1) and Equations (24), (25) and (B3) of [31] by means of simulation code. The accuracy of the numerical results is confirmed by other independent code developed for this purpose.

3.2. Eventual contributions from the minority carriers

For the DOS model of Figure 4 the DOS above E_F is much lower than that below E_F such that $\tau_{\omega n} \gg \tau_{\omega p}$. In our simulations, it is considered that $\mu_n = 10\mu_p$, so that the mobility capture time product of electrons dominates, namely $\mu_n \tau_{\omega n} \gg \mu_p \tau_{\omega p}$. This ensures that $Y \cong Y_n$, as is evident in Figure 5a. This can be experimentally confirmed from the fact that the Y signal at higher ω is independent of the bias light level, because the function H is unity. By contrast, the experimental Y signal at higher ω is expected to depend on the bias light level in the cases where the Y signal differs from the imaginary part for the majority carriers Y_n for $\mu_n \tau_{\omega n} \leq \mu_p \tau_{\omega p}$, as a result of mixed contributions from the electrons and holes. These are shown in the example of Figure 5b obtained upon increasing the mobility of holes at $\mu_p = 10^2 \mu_n$ and that of Figure 5c obtained upon decreasing both capture coefficients c_p^v and c_n^v of the $D^v(E)$ by a factor of 10^3 lower than the values introduced above so that $\tau_{\omega n} \approx \tau_{\omega p}$. Therefore, the behavior of the experimental Y spectra at higher ω can be used to

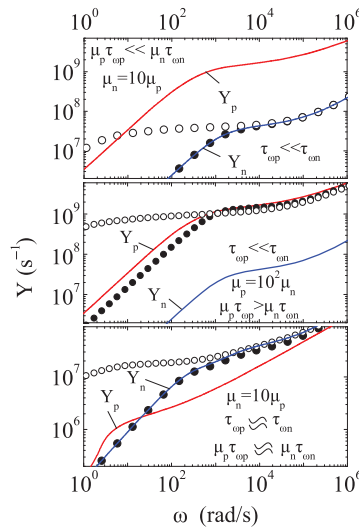


Figure 5. Calculated Y spectra for a low $n_0 = 1.1 \times 10^7 \text{ cm}^{-3}$ (open symbols) and moderate $n = 1 \times 10^{10} \text{ cm}^{-3}$ (solid symbols) for $\mu_n = 10 \text{ cm}^2 \text{ V}^{-1} \text{ s}^{-1}$ using the DOS model of Figure 4 by setting $\mu_p = 0.1\mu_n$ in (a), $\mu_p = 10^2\mu_n$ in (b), and the relatively lower capture coefficients $c_p^v = 10c_n^v = 1 \times 10^{-10} \text{ cm}^3 \text{ s}^{-1}$ and $\mu_p = 0.1\mu_n$ in (c). The respective Y_n and Y_p spectra calculated for the moderate n are included for comparison.

conclude whether these spectra are dominated or not by the imaginary part of the majority carriers (Y_n).

3.3. Contributions from the probed and recombination states

The behavior of the Y signal according to Equation (18) may depend on the parameter C_e when electrons dominate. This is confirmed in the examples of Figure 6a calculated for a fixed $n = 1 \times 10^{10} \text{ cm}^{-3}$ and different C_e obtained upon introducing different values for c_n^v . Specifically, for $C_e < 0.5$ the Y signal has a negligible dependence on C_e in agreement with Equation (18), and Y practically agrees with the $1/\tau_{\omega n}$ rate calculated from Equation (12). This is illustrated in Figure 7a, which presents Y spectra calculated for $C_e = 0.1$ and generation rates G_{dc} ranging from 2.2×10^{13} to $2.2 \times 10^{18} \text{ cm}^{-3} \text{ s}^{-1}$. The characteristic light intensity-dependent decay of the Y spectra at low ω can be seen. This behavior is also usually observed experimentally (see Figure 10a below) and it can be an indication that the trap-limited conduction mechanism predominates over the alternative hopping transport [46]. Each characteristic decay of the Y signal in Figure 7a (solid lines) is in excellent agreement with that of the $1/\tau_{\omega n}$ rate (triangles) calculated from Equation (12). As shown in the example of Figure 7a with $n = 10^{10} \text{ cm}^{-3}$, Y_{2n} is negative. At low ω , Y_{3n} is positive and counteracts a

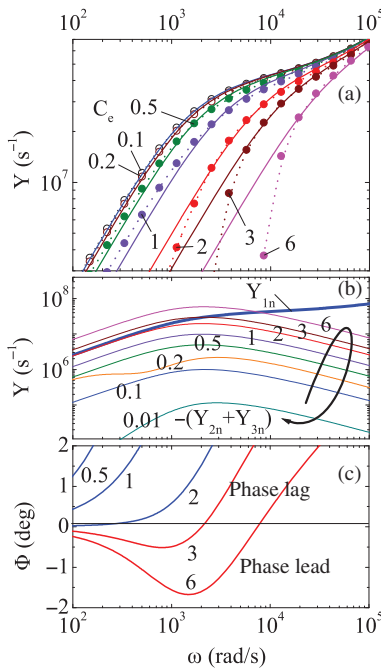


Figure 6. (a) Y spectra (circles and dotted lines) calculated for $n = 1 \times 10^{10} \text{ cm}^{-3}$ and the indicated values of C_e in comparison with the respective reconstructed $1/\tau_{\omega n}$ rates (solid lines). (b) Comparison of the Y_{1n} spectrum (thick solid line) with the spectra of the total negative $Y_{2n} + Y_{3n}$ contribution (thin solid lines) for the indicated C_e (numbers). (c) Examples of phase shift lag ($\phi > 0$) and phase shift lead ($\phi < 0$) spectra obtained for the indicated C_e (numbers).

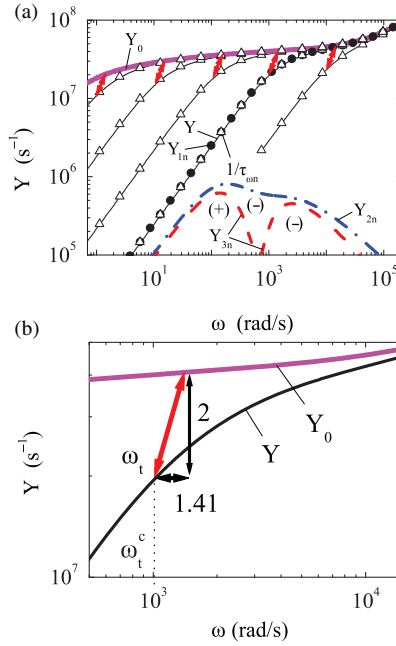


Figure 7. (a) Calculated spectra of Y (solid lines) and $1/\tau_{\omega n}$ (open triangles) of different densities n (2.9×10^6 , 10^7 , 10^8 , 10^9 , 10^{10} and 10^{11} cm^{-3} from left to right in the figure). Y_{1n} spectrum (solid circles) in comparison with Y_{2n} (dashed-dotted lines) and Y_{3n} (dashed lines) spectra for the moderate $n = 10^{10} \text{ cm}^{-3}$. The signs of Y_{2n} and Y_{3n} are indicated. The bias light-independent Y_0 spectrum (thick solid line) is obtained with a near dark equilibrium density $n_0 = 2.9 \times 10^6 \text{ cm}^{-3}$. (b) An example demonstrating the determination of ω_t for the Y signal of $n = 10^{10} \text{ cm}^{-3}$. ω_t is defined as the frequency where the Y signal decreases by a factor of 2 (vertical double arrow) from the respective value in the Y_0 spectrum of the same trap depth which is, by a factor of 1.41 (horizontal double arrow), above ω_t .

significant part of Y_{2n} , so that $Y_{2n} + Y_{3n}$ is suppressed at very low negative values (see Figure 6b). This assures that Y_{1n} dominates in Y_n , in very good agreement with the prediction of Equation (18).

Upon increasing C_e , the majority carrier lifetime decreases with only a minor change in the minority carrier lifetime, in very good agreement with the predictions of Equations (15) and (16), respectively, as confirmed in Figure 8a. This way, as shown in Figure 8b, the relative density of free holes increases compared to that of free electrons, which is kept fixed. In addition, the exact K_{re} agrees with the approximate K_{re} and their small difference from the p/n ratio, which is not detectable in the graphs of Figure 8b, is in good agreement with Equation (25). In this figure, the recombination rate, R , increases with C_e , according to the prediction of Equation (17). This way, the contributions from the Y_{2n} and Y_{3n} components, which are proportional to the recombination rates of free electrons with trapped holes, both become negative for $C_e \geq 0.5$ and increase upon increasing C_e . This is confirmed in Figure 6b where, for $C_e \geq 0.5$, the maximum of $-(Y_{2n} + Y_{3n})$ around $\omega_t^c = 10^3 \text{ rad s}^{-1}$ becomes comparable to Y_{1n} . Thus, the Y signal in Figure 6a starts to decay from

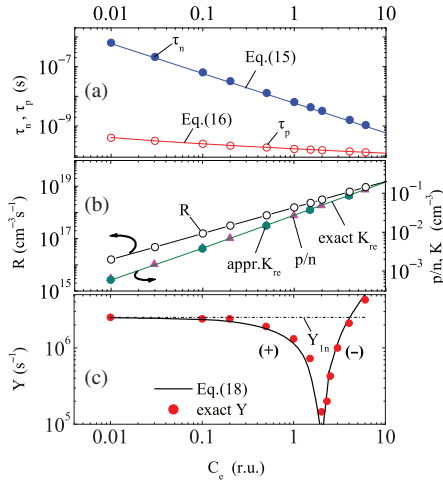


Figure 8. Exact lifetimes τ_n and τ_p and approximate lifetimes from Equations (15) and (16) in (a), recombination rate R , p/n ratio, exact K_{re} from Equation (23) and approximate K_{re} from Equation (25) in (b) and calculated exact Y signal (solid circles) in comparison with Y signal (solid line) calculated from Equation (18) in the LF regime ($\omega=98 \text{ rad s}^{-1}$) in (c) for a constant $n = 10^{10} \text{ cm}^{-3}$ as a function of C_e .

gradually higher frequencies upon increasing C_e and becomes lower than Y_{1n} according to Equation (18). This is quantitatively confirmed in Figure 8c where the exact Y signal (solid circles) in the LF regime calculated for $\omega = 98 \text{ rad s}^{-1}$ and various C_e is in excellent agreement with the prediction of Equation (18) (solid line). It is worth mentioning that as C_e increases, the restriction $nc_n^i \gg pc_p^i$ used to derive Equation (18) may not be valid, particularly at higher C_e . In this case, it was found that only the trend of Y_n is qualitatively described by Equation (18).

Around $C_e = 2$ a characteristic change in the sign of the Y signal of the LF regime is predicted from Equation (18) so that, for $C_e > 2$, it becomes negative. Remarkably, very similar behavior is also confirmed in the examples of the exact Y signal for $C_e > 2$ of Figure 8c. In this case, the total negative contribution from $Y_{2n} + Y_{3n}$ exceeds that of Y_{1n} around $\omega_i^c = 10^3 \text{ rad s}^{-1}$ and lower ω (see Figure 6b). Thus, the phase lead from the Y_{2n} and Y_{3n} components dominates over the phase lag from Y_{1n} at low ω , as shown in the phase shift spectra of Figure 6c with $C_e = 3$ and 6. In this case, i_{ac} is ahead of the modulated light (see Figure 1b). This does not mean that the MPC in the output anticipates the modulated light in the input. In fact, as long as the periodic oscillations of the illumination continue unchanged, the MPC is influenced at some finite time in the past by the recombination processes involved in Y_{2n} and Y_{3n} inducing the phase lead.

3.4. Determination of the relative contributions to the Y signal and of the DOS parameters

The above analysis showed that only for $C_e < 0.5$ are the contributions to the Y signal from the recombination practically negligible so that reliable DOS parameters can

be extracted. This possibility, as predicted above, can be experimentally verified by comparing the decay of the experimental Y signal around ω_t with that of the $1/\tau_{\omega n}$ rate. Therefore, the determination of this rate is crucial. It can be calculated from Equation (12) by means of ω_t and $D(E)$, which can be reconstructed from the experimental Y spectra, as illustrated below with the aid of simulations. We call the rate so-calculated, the $1/\tau_{\omega}$ rate, as it is a reconstruction of the actual $1/\tau_{\omega n}$.

The ω_t required for the calculation of $1/\tau_{\omega}$ from Equation (12) can be determined according to the procedure presented earlier [31,33,35] which is illustrated with the aid of the simulated example of Figure 7b. This procedure takes advantage of the fact that for $\omega = \omega_t$ the function H becomes $1/2$. This is experimentally evident as a decay in the Y signal by a factor of 2 (vertical arrow) with respect to the value of the Y_0 spectrum with the same trap depth, which corresponds to a frequency higher than ω_t by a factor of $\sqrt{2} = 1.41$ (horizontal arrow). This is because the trap depth of Y , obtained from Equation (20) for $\omega = \omega_t$, is obtained in the Y_0 spectrum by using $\omega = \sqrt{2}\omega_t$ in Equation (20), as the characteristic frequency of Y_0 appearing in the denominator of the above equation is practically zero. The so-determined ω_t in the example of Figure 7b, obtained with $C_e = 0.1$, is in excellent agreement with the actual characteristic frequency ω_t^c (dotted line). From the so-derived ω_t , the capture coefficient c_n , and $H(\omega, \omega_t)$ are obtained, which are introduced in Equation (12) to calculate the $1/\tau_{\omega}$ rate. It is worth mentioning that, for the accurate determination of ω_t , it is essential to obtain the Y_0 spectrum. The Y_0 in the examples of Figures 7a and 7b is obtained with an electron density n_0 near dark equilibrium ($n_0 = 2.9 \times 10^6 \text{ cm}^{-3}$). Unfortunately, under this condition the Y_0 spectrum cannot be obtained experimentally at sufficiently high frequencies. As can be seen from Figure 7a, the Y_0 spectrum coincides with the upper envelope in which the Y spectra of different bias light levels merge, because, in this envelope, $H(\omega, \omega_t) \cong 1$. So this envelope can be safely used to experimentally determine Y_0 .

Finally, the $D(E)$ parameter required in Equation (12) can be obtained from the best fit to the bias light-independent Y_0 spectrum (upper envelope of the Y spectra) using $Y_0 \cong \frac{\pi}{2} c_n D(E_{\omega n}) kT$. This requires us to convert the probe trap depths ($E_{\omega n}$) of $D(E)$ into the respective frequencies by means of Equation (20) as follows. In the denominator of this equation, the respective ω_t for Y_0 is negligible. In the numerator, the μN_0 product can be assumed if it is unknown. For the parameters ω_t and σ_p appearing also in the numerator, the respective values of a moderate bias light level can be used. These values are those from which c_n is calculated. As $D(E)$ is determined, it can be introduced into Equation (12) to calculate the $1/\tau_{\omega}$ rate by means of ω_t . Specifically, the extracted ω_t of a given bias light level is used to determine, for any ω , the respective probe trap depth $E_{\omega n}$ from Equation (20) and to specify the respective $D(E_{\omega n})$, which is introduced in Equation (12).

Upon applying this procedure, the $1/\tau_{\omega}$ rates are reconstructed for all the examples of Y spectra of different C_e , which can possibly be observed experimentally. These rates are plotted in Figure 6a (solid lines). In this figure, it can be seen that the respective Y signal of Figure 6a, obtained for $C_e < 0.5$ (open circles and dotted lines), where the total contribution from Y_{2n} and Y_{3n} is practically negligible (see Figure 6b), agrees with the respective reconstructed $1/\tau_{\omega}$ rate. If such behavior is experimentally observed, it can be safely concluded that C_e is relatively low, which provides a low recombination rate, such that $1/\tau_{\omega} \cong 1/\tau_{\omega n}$. In this case, by applying

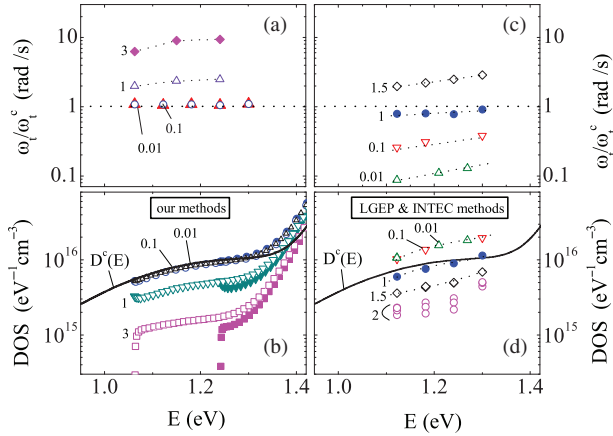


Figure 9. Normalized reconstructed characteristic frequency ω_t/ω_t^c in (a) and (c) and reconstructed $D(E)$ (symbols) in comparison with the introduced $D^c(E)$ (solid line) in (b) and (d) as a function of the energy for the indicated C_e (numbers), according to our methods (a) and (b) and the methods of the LGEP and INTEC groups (c) and (d).

our methods, the actual characteristic frequency and the actual DOS from Equation (19) are successfully reconstructed. This is confirmed in the examples of Figures 9a and b with $C_e < 0.5$ where it is found that $\omega_t/\omega_t^c \cong 1$ and $D(E) \cong D^c(E)$, respectively. By contrast, the Y signal in the examples of Figure 6a, obtained for $C_e \geq 0.5$ (solid circles and dotted lines), systematically differs from the respective reconstructed $1/\tau_\omega$ rate. Such experimental behavior can be used to safely conclude that $1/\tau_\omega$ differs from the actual $1/\tau_{\omega n}$ and our methods cannot provide the actual DOS parameters. This is due to the relatively high C_e and recombination rate so that $Y_{2n} + Y_{3n}$ is not negligible (see Figure 6b). Indeed, in the examples with $C_e \geq 0.5$, ω_t in Figure 9a significantly overestimates ω_t^c ($\omega_t/\omega_t^c > 1$), whereas in Figure 9b, $D(E)$ calculated from Equation (19) significantly underestimates $D^c(E)$ and does not overlap for different bias light intensities.

We have also applied the methods of the LGEP and INTEC groups to the respective MPC data of the LF regime obtained with the DOS model of Figure 4. The characteristic frequency ω_t , according to the method proposed by the authors of the above groups [41], is obtained from the frequency where the DOS calculated from Equation (22) deviates 10% from the respective constant value of the LF regime. This requires us to obtain a single DOS value from Equation (22) by means of all the phase shift data in the LF regime. However, such a single DOS value for every energy is only achieved for $C_e < 2$, as is evident from Figure 9(d). For $C_e \geq 2$ the Y signal presents a steeper decay than the linear decay (see Figure 6a). Thus at every energy, Equation (22) gives different values for the DOS by means of the phase shift values of low ω , as in the example of Figure 9(d) for $C_e = 2$. The so-derived DOS parameters in Figures 9(c) and (d) are close to the actual ones, exclusively for the MPC data of the case of $C_e = 1$, which cannot be experimentally verified. For $C_e < 1$ or $C_e > 1$ the methods of LGEP and INTEC groups cannot provide the actual DOS parameters, as predicted in Section 2.

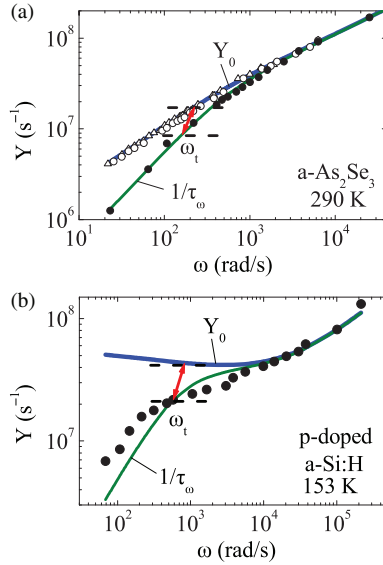


Figure 10. (a) Experimental spectra of the Y signal of a-As₂Se₃ sputtered films taken from our previous publication [35] for light intensities of 8.2×10^{11} (open triangles), 3.6×10^{12} (open circles) and 2.8×10^{13} (solid circles) $\text{cm}^{-2} \text{s}^{-1}$. (b) Experimental spectra of the Y and Y_0 spectra extracted from the MPC data of light p-type doped a-Si:H reported by Kleider et al. [24]. Each reconstructed $1/\tau_\omega$ rate (solid line) is also included in (a) and (b) for comparison.

4. Comparison with experimental results

A typical experimental example of Y spectra, which are obtained from the analysis of our MPC data of a-As₂Se₃ sputtered films taken from Figure 1 of [35], is presented in Figure 10a. The two Y signals of weak bias illumination levels (open symbols) and the Y signal at higher ω of the moderate bias light level (solid symbols) merge into a single line, defining the bias light intensity-independent Y_0 spectrum. The decay at lower ω of the experimental Y spectrum of the moderate bias light level agrees with the characteristic decay of the $1/\tau_\omega$ rate, reconstructed by means of the Y spectra and Equation (12) following the procedure described in Section 2.4. This agreement is an experimental verification of Equation (12) predicted for low $C_{h,e}$ when unipolar conduction by the majority carriers dominates. Unipolar conduction is indeed taking place by holes [47] in a-As₂Se₃. Moreover, the above films are characterized by a high photosensitivity with a high photo-to-dark current ratio of the order of 10^3 , which is compatible with a low C_h . Therefore, the interaction of holes with the probed states dominates in the Y signal of a-As₂Se₃ and the previously extracted [35] DOS parameters from this signal by applying our methods are reliable.

Another characteristic example of an experimental Y signal is presented in Figure 10b. This is obtained from the DOS reported by Kleider et al. [24], as calculated from the MPC data of a lightly p-type doped a-Si:H sample. Specifically, the Y spectrum is extracted from the DOS presented in Figure 24a of [24] which was calculated by means of the formula of Bruggenann et al. [6]. This formula is equivalent to our Equation (19) with $H(\omega, \omega_t) = 1$ from which it is evident that the

calculated DOS is proportional to Y . Hence this DOS also reflects the Y signal in the energy domain E_ω . By adopting the relation $E_\omega = kT \ln(\nu_0/\omega)$ with $\nu_0 = 10^{12} \text{ s}^{-1}$, used by Kleider et al. to define the energy scale, the Y signal extracted from the DOS data is converted into the frequency domain ω . The result is presented in Figure 10b along with the Y_0 spectrum, which is extracted from the upper envelope of the DOS's of different temperatures. It can be seen that the Y signal clearly departs from the $1/\tau_\omega$ rate, reconstructed according to the procedure described in Section 2.4. This is the predicted behavior for the case where the Y signal is not dominated by the interaction of the majority carriers with the probed states. This conclusion is reasonable for this lightly doped material in which mixed contributions from both carriers are expected, making it impossible to extract a DOS.

5. Conclusions

We have obtained general exact expressions for the Y signal without any approximation, which clarify all the physical processes involved in the Y signal. It was illustrated how the predominant process of these physical processes can be experimentally detected, by means of examples of simulations and experimental data. Specifically, it was found that mixed contributions from the recombination of free majority carriers with trapped minority carriers may dominate in the Y signal of lower ω and may induce a phase lead, complicating the extraction of a DOS. This is obtained as long as the capture coefficient for the majority carriers of the recombination centers where the minority carriers are trapped is comparable to or higher than that of the recombination centers where the majority carriers are trapped, that is for $C_{e,h} \geq 0.5$. This condition for a given DOS favors a relatively lower lifetime for the majority carriers and higher recombination rate. By contrast, for $C_{e,h} < 0.5$, the mixed contributions from the recombination are negligible, so that the contribution from the capture rate of the majority carriers into the probed states dominates in the Y signal. This can be verified experimentally, because the above capture rate can be reconstructed from the experimental Y spectra. If the reconstructed $1/\tau_\omega$ rate agrees with the Y signal, then this rate dominates in the Y signal and the accurate DOS parameters can be obtained with confidence by our DOS spectroscopy. It was shown that the methods reported by the LGEP and INTEC groups are reliable exclusively for $C_{e,h} = 1$, which unfortunately cannot be verified experimentally.

References

- [1] H. Oheda, J. Appl. Phys. 52 (1981) p.6693.
- [2] H. Oheda, H. Okushi, H. Tokumaru and K. Tanaka, Jpn. J. Appl. Phys. 20 (1981) p.L689.
- [3] C. Longeaud, J.P. Kleider and M. Cuniot, Opt. Mater. A 294–296 (2000) p.519.
- [4] H. Oheda, S. Yamasaki, T. Yoshida, A. Matsuda, H. Okushi and K. Tanaka, Jpn. J. Appl. Phys. 21 (1982) p.L440.
- [5] G. Schumm and G. Bauer, Phil. Mag. B 58 (1988) p.411.
- [6] R. Bruggemann, C. Main, J. Berkin and S. Reynolds, Phil. Mag. B 62 (1990) p.29.
- [7] P. Kounavis and E. Mytilineou, J. Non-Cryst. Solids 137–138 (1991) p.955.

- [8] J.P. Kleider, C. Longeaud and O. Glodt, *J. Non-Cryst. Solids* 137–138 (1991) p.447.
- [9] C. Main, D.P. Webb, R. Bruggemann and S. Reynolds, *J. Non-Cryst. Solids* 137–137 (1991) p.951.
- [10] P. Kounavis, *J. Non-Cryst. Solids* 352 (2006) p.1068.
- [11] R. Bruggemann, *J. Mater. Sci. Mater. Electron.* 14 (2003) p.629.
- [12] M. Takeda, R. Tamura, Y. Sakairi and K. Kimura, *J. Solid State Chem.* 133 (1997) p.224.
- [13] T. Tanaka, M. Mazu and R. Hiroasi, *Thin Solid Films* 322 (1998) p.290.
- [14] M. Breban, P.B. Romero, S. Mezheny, V.W. Bollarotto and E.D. Williams, *Appl. Phys. Lett.* 87 (2005) p.203503.
- [15] S. Reynolds, Z. Aneva, Z. Levi, D. Nesheva, C. Main and V. Smirnov, *J. Non-Cryst. Solids* 354 (2008) p.2744.
- [16] G. Schumm and G. Bauer, *Phys. Rev. B* 39 (1989) p.5311.
- [17] P. Kounavis and E. Mytilineou, *J. Non-Cryst. Solids* 201 (1996) p.119.
- [18] P. Grygiel and W. Tomaszewicz, *J. Phys. Condens. Matt.* 12 (2000) p.5209.
- [19] J.P. Kleider and C. Longeaud, *Phys. Rev. B* 45 (1992) p.11672.
- [20] K. Hattori, Y. Adachi, M. Anzai, H. Okamoto and Y. Hamakawa, *J. Appl. Phys.* 76 (1994) p.2841.
- [21] P. Kounavis and E. Mytilineou, *J. Non-Cryst. Solids* 164–166 (1993) p.623.
- [22] P. Kounavis, *J. Appl. Phys.* 77 (1995) p.3872.
- [23] P. Kounavis and E. Mytilineou, *Solid State Phenom.* 44–46 (1995) p.715.
- [24] J.P. Kleider and C. Longeaud, *Solid State Phenom.* 44–46 (1995) p.596.
- [25] P. Kounavis, D. Mataras and D. Rapakoulias, *J. Appl. Phys.* 80 (1996) p.2305.
- [26] P. Kounavis and E. Mytilineou, *Phil. Mag. Lett.* 72 (1996) p.117.
- [27] W. Lauwerence, PhD thesis, University of Leuven, 1997.
- [28] S. Reynolds, C. Main, D.P. Webb and M.J. Rose, *Phil. Mag. B* 80 (2000) p.547.
- [29] R. Bruggemann and J.P. Kleider, *Thin Solid Films* 403–404 (2002) p.30.
- [30] J.P. Kleider, C. Longeaud and M.E. Guenier, *Phys. Status Solidi (c)* 1 (2004) p.1208.
- [31] P. Kounavis, *Phys. Rev. B* 64 (2001) p.45204.
- [32] P. Kounavis, *Phys. Rev. B* 65 (2002) p.155207.
- [33] P. Kounavis, *J. Non-Cryst. Solids* 326–327 (2003) p.98.
- [34] P. Kounavis, *Rec. Devel. Phys. (Transworld Research Network)* 4 (2003) p.773.
- [35] P. Kounavis, *Sol. State Commun.* 131 (2004) p.47.
- [36] P. Kounavis, *J. Appl. Phys.* 97 (2005) p.23707.
- [37] R.R. Koropecski, J.A. Schmidt and R. Arce, *J. Appl. Phys.* 91 (2002) p.8965.
- [38] M.E. Guenier, C. Longeaud and J.P. Kleider, *Eur. Phys. J. Appl. Phys.* 26 (2004) p.75.
- [39] C. Longeaud, J.A. Schmidt and J.P. Kleider, *Phys. Rev. B* 73 (2006) p.235316.
- [40] J.A. Schmidt, C. Longeaud, R.R. Koropecski and R. Arce, *J. Appl. Phys.* 101 (2007) p.103705.
- [41] J.A. Schmidt, C. Longeaud, R.R. Koropecski and R. Arce, *J. Non-Cryst. Solids* 354 (2008) p.2914.
- [42] M. Pomoni, A. Giannopoulou and P. Kounavis, *J. Non-Cryst. Solids* 354 (2008) p.2238.
- [43] G.W. Taylor and J.G. Simmons, *J. Non-Cryst. Solids* 8–10 (1972) p.940.
- [44] J. Bullo, P. Cordier, M. Gauthier and G. Mawawa, *Phil. Mag.* 55 (1987) p.599.
- [45] R.H. Bube, *Photoconductivity of Solids*, John Wiley, New York, 1960.
- [46] C. Longeaud and S. Tobbeche, *J. Phys. Condens. Matter* 21 (2009) p.045508.
- [47] R.A. Street, *Phil. Mag. B* 38 (1978) p.191.
- [48] J.P. Kleider, C. Longeaud and M.E. Guenier, *J. Non-Cryst. Solids* 338–340 (2004) p.390.

Appendix. Approximate expression for K

The general expression for K appearing in the exact expression for n_{ac} derived in our first analysis [31] (see Equation (B3) of [31]) is given by

$$K = \frac{1 + \sum_i \int_{E_V}^{E_C} \frac{1}{j\omega + S^i(E)} \frac{pc_p^i + r_p^i(E)}{S^i(E)} c_n^i D^i(E) dE}{1 + \sum_i \int_{E_V}^{E_C} \frac{1}{j\omega + S^i(E)} \frac{nc_n^i + r_n^i(E)}{S^i(E)} c_p^i D^i(E) dE}. \quad (23)$$

This expression is simplified in the LF regime ($\omega \ll \omega_i^j$) for the case where the gap state distribution $D^c(E)$ dominates above E_F and another gap state distribution $D^v(E)$ dominates below E_F . In the imaginary parts and the real parts of the numerator and denominator of Equation (23), some integrals are obtained which are reduced as follows: specifically, the obtained integrals $\int_{E_V}^{E_C} b_{\omega n, p}^{v, c}(E) c_{n, p}^{v, c} D^{v, c}(E) dE$ can, to a good approximation, be replaced by $\frac{\pi}{2} H(\omega, \omega_i^{v, c}) c_n^{v, c} D(E_{\omega n, p}) kT$; in the LF regime the probe energy levels $E_{\omega n, p}^{v, c}$ are practically fixed at the respective trap quasi-Fermi levels $E_{\omega n, p}^{v, c} \cong E_{in, p}^{v, c}$ and the H function is approximated as $H(\omega, \omega_i^{v, c}) \cong \frac{2}{\pi} \frac{\omega}{\omega_i^{v, c}}$, so that the above integrals become $\frac{\omega}{\omega_i^{v, c}} c_{n, p}^{v, c} N_{in, p}^{v, c}$, where $N_{in, p}^{v, c} = D(E_{in, p}^{v, c}) kT$; finally, the obtained integrals

$$\int_{E_V}^{E_C} \frac{b_{\omega n, p}^{v, c}(E)}{S^{v, c}(E)} c_{n, p}^{v, c} D^{v, c}(E) dE$$

can be approximated by

$$\frac{\omega}{2(\omega_i^{v, c})^2} c_{n, p}^{v, c} N_{in, p}^{v, c}.$$

Upon incorporating the charge neutrality condition (Equation (13)) presented in Section 2 and defining $g_n = N_{in}^c / N_r^c$ and $g_p = N_{ip}^v / N_r^v$, the expression for K becomes

$$K \cong \frac{-j\omega(\frac{1}{\omega_i^c} + \frac{1}{2\omega_i^c} g_n) + (1 + g_n)}{-j\omega(\frac{1}{\omega_i^v} + \frac{1}{2\omega_i^v} g_p) + (1 + g_p)} \left(\frac{p}{n}\right). \quad (24)$$

From the above relation the real and imaginary parts of K are obtained for the LF regime in the simple forms

$$K_{re} \cong \alpha_{re} \frac{p}{n}, \quad (25)$$

$$K_{im} \cong \frac{\omega}{\omega_i^v} \alpha_{im} \frac{p}{n}, \quad (26)$$

where

$$\alpha_{re} = \frac{1 + g_n}{1 + g_p}, \quad (27)$$

$$\alpha_{im} = \frac{(1 + g_n)(1 + \frac{g_p}{2}) - (1 + \frac{g_n}{2} \frac{c_n^v}{c_p^v})(1 + g_p)}{(1 + g_p)^2}. \quad (28)$$

The parameter α_{re} given by Equation (27) is usually close to unity for smooth gap state distributions above and below E_F , providing that the quasi-Fermi levels are separated by more than a few kT .